A Robust seventh-order WENO Scheme and its applications

Article · January 2008

DOI: 10.2514/6.2008-757

2 authors:

Yiqing Shen
Chinese Academy of Sciences
52 PUBLICATIONS **853** CITATIONS
SEE PROFILE

Gecheng Zha
University of Miami
224 PUBLICATIONS **2,628** CITATIONS
SEE PROFILE

A Robust Seventh-order WENO Scheme and Its Applications

Yiqing Shen*, Gecheng Zha†
Dept. of Mechanical and Aerospace Engineering
University of Miami
Coral Gables, Florida 33124
E-mail: yqshen@miami.edu, gzha@miami.edu

Abstract

This paper has analyzed the seventh-order WENO scheme of Balsara and Shu[1] and designed the improved weights for a new seventh-order WENO scheme. The new scheme can not only keep the essentially non-oscillatory property, but can also obtain higher accuracy in smooth regions. Some detailed numerical results are present.

1 Introduction

The direct numerical simulation and large-eddy simulation of transonic compressible turbulent flows require the use of highly accurate numerical schemes, which must be capable of capturing shock waves and resolving a broad range of length scales. The high order weighted essentially non-oscillatory(WENO) schemes are designed for this purpose and are the primary schemes used as the current state of the art.

The WENO schemes were originally proposed by Liu et al [2], and have been improved by Jiang and Shu[3]. In the past decade, there are various improvements and applications of WENO schemes. Shu[4] summarized the main features of different WENO schemes for their applicabilities and strengths.

There are two active areas for WENO schemes development. One is to improve the ENO properties, for example, Wang and Chen [5] proposed optimized WENO schemes for linear waves with discontinuity; Panziani et al [6] developed the optimized WENO schemes to improve the resolution of a class of compressible flows characterized by a wide disparity of scales for compressible turbulence and/or aeroacoustic phenomena, and shock waves; Balsara and Shu[1] developed the monotonicity preserving WENO schemes; Xu and Shu[7] generalized a technique of anti-diffusive flux corrections to WENO schemes; Henric[8] used a mapped-WENO to achieve optimal order near critical points. The other area is to combine WENO with other high order schemes, for example, Pirozzoli[9] proposed a hybrid compact-WENO scheme for shock-turbulence interaction; Kim and Kwon[10] proposed a high-order accurate hybrid scheme using a central flux scheme and a WENO scheme for compressible flowfield analysis, Shen and Yang[11] developed hybrid finite compact-WENO schemes.

Latini et al [12] studied the effects of WENO flux reconstruction order and spatial resolution on reshocked two-dimensional Richtmyer-Meshkov instability. It is shown that higher-order higher-resolution

* Research Scientist, AIAA Member
† Associate Professor, AIAA Senior Member

simulations have lower numerical dissipation. Lower-order simulations preserve large-scale structures and flow symmetry, while higher-order higher-resolution simulations exhibit fragmentation of the structures, symmetry breaking and increased mixing. Their computational scaling shows that increasing the order is more advantageous than increasing the resolution for the flow.

However, the majority of the WENO scheme development and application has been limited to the order of accuracy lower than 5th order. A class of higher than 5th order weighted essentially non-oscillatory schemes are designed by Balsara and Shu in [1]. The order of these WENO schemes are from seven to eleven. In this paper, we analyze the smoothness estimators suggested by Balsara and Shu for their seventh-order WENO schemes and improve the smooth estimator by making them more uniform in smooth regions. Such improvement achieves better accuracy in the smooth regions than the original B-S 7th order WENO scheme. Numerical examples show that the new 7th order WENO scheme is accurate and robust.

2 The seven-order WENO scheme

For the hyperbolic conservation law

$$\frac{\partial u}{\partial t} + \frac{\partial f(u)}{\partial x} = 0, \tag{1}$$

The semi-discrete conservative difference equation of Eq.(1) can be written as

$$\frac{du_i}{dt} = -\frac{1}{\Delta x}(f_{i+\frac{1}{2}} - f_{i-\frac{1}{2}}) \tag{2}$$

where $f_{i+\frac{1}{2}}$ is the numerical flux, $f_{i+\frac{1}{2}} = f(u^L_{i+\frac{1}{2}}, u^R_{i+\frac{1}{2}})$. In this paper, the high order accuracy of the flux $f_{i+\frac{1}{2}}$ is achieved by using high order interpolation of the conservative variables $u^L_{i+1/2}$ and $u^R_{i+1/2}$, which follows the same principle suggested by Van Leer [13].

2.1 The ENO scheme

In this paper, only the reconstruction of $u^L_{i+1/2}$ is discussed as the example, the $u^R_{i+1/2}$ is symmetric with respect to $x_{i+1/2}$ and will not be derived to save the space.

The rth-order ENO scheme chooses the smoothest stencil from r candidate stencils and uses the chosen stencil to approximate the flux $h_{i+1/2}$. Let's denote the r candidate stencils by S_k, $k = 0, ..., r-1$, where

$$S_k = (x_{i+k-r+1}, x_{i+k-r+2}, \cdots, x_{i+k})$$

If the stencil S_k is chosen as the smoothest interpolation stencil following the procedure given by Jiang and Shu[3], then the numerical flux of the rth-order ENO scheme is

$$u^L_{i+\frac{1}{2}} = q_k(u_{i+k-r+1}, u_{i+k-r+2}, \cdots, u_{i+k})$$

where

$$q_k(u_{i+k-r+1}, u_{i+k-r+2}, \cdots, u_{i+k}) = \sum_{l=0}^{r-1} \alpha_{k,l} u_{i+k-l}$$

2.2 The WENO scheme

The WENO scheme uses a convex combination of all the candidates stencils instead of the "smoothest" one adopted in the ENO scheme. Each of the candidate stencils is assigned a weight, which determines the

contribution of this stencil to the final approximation of the numerical flux. The weights can be defined in such a way that in smooth regions it approaches the optimal weights to achieve a high order accuracy with minimum dissipation due to symmetric interpolation of the variables, while in regions near discontinuities, the stencils that contain the discontinuities are assigned a nearly zero weight to shift the scheme to one-side differencing. The final numerical flux can be written as

$$u^L_{i+\frac{1}{2}} = \sum_{k=0}^{r-1} \omega_k q_k(u_{i+k-r+1}, u_{i+k-r+2}, \cdots, u_{i+k}) \tag{3}$$

The weight ω_k is defined as

$$\omega_k = \frac{\alpha_k}{\alpha_0 + \cdots + \alpha_{r-1}},$$

where

$$\alpha_k = \frac{C_k}{(\epsilon + IS_k)^p}, k = 0, 1, \cdots, r-1 \tag{4}$$

where ϵ is a small positive real number introduced to avoid the denominator becoming zero; C_k are the optimal weight coefficients given by Balsara and Shu in [1]. IS_k is the smoothness measurement of the flux function on the kth candidate stencil. These parameters ϵ, p, and IS_k can affect the performance of WENO scheme. The smoothness measurement proposed by Liu et al.[2] gives a fourth-order accurate WENO; Jiang and Shu[3] define the IS_k as Eq.(5). They obtained the optimal fifth-order accurate WENO scheme when $r = 3$. Liu et al.[14] used a small positive number p for smooth area and a large p near discontinuities region. Shen et al.[15] found the ϵ value can affect the converging efficiency for steady state flow calculation.

$$IS_k = \sum_{l=1}^{r-1} \int_{x_{i-1/2}}^{x_{i+1/2}} h^{2l-1} (p_k^{(l)})^2 dx \tag{5}$$

where $p_k^{(l)}$ is the lth-order derivative of $p_k(x)$.

2.3 The seventh-order WENO scheme of Balsara and Shu[1]

For the seventh-order WENO scheme ($r = 4$) of Balsara and Shu[1](B-S WENO-7), the fourth-order interpolations $q_k(\ k = 0, \cdots, 3)$ are

$$\begin{aligned}
q_0 &= -\tfrac{1}{4}u_{i-3} + \tfrac{13}{12}u_{i-2} - \tfrac{23}{12}u_{i-1} + \tfrac{25}{12}u_i \\
q_1 &= \tfrac{1}{12}u_{i-2} - \tfrac{5}{12}u_{i-1} + \tfrac{13}{12}u_i + \tfrac{1}{4}u_{i+1} \\
q_2 &= -\tfrac{1}{12}u_{i-1} + \tfrac{7}{12}u_i + \tfrac{7}{12}u_{i+1} - \tfrac{1}{12}u_{i+2} \\
q_3 &= \tfrac{1}{4}u_i + \tfrac{13}{12}u_{i+1} - \tfrac{5}{12}u_{i+2} + \tfrac{1}{12}u_{i+3}
\end{aligned} \tag{6}$$

and the smoothness estimators given by Balsara and Shu[1] are

$$\begin{aligned}
IS_0^4 = \;& u_{i-3}(547u_{i-3} - 3882u_{i-2} + 4642u_{i-1} - 1854u_i) + u_{i-2}(7043u_{i-2} - 17246u_{i-1} \\
& +7042u_i) + u_{i-1}(11003u_{i-1} - 9402u_i) + 2107u_i^2 \\
IS_1^4 = \;& u_{i-2}(267u_{i-2} - 1642u_{i-1} + 1602u_i - 494u_{i+1}) + u_{i-1}(2843u_{i-1} - 5966u_i \\
& +1922u_{i+1}) + u_i(3443u_i - 2522u_{i+1}) + 547u_{i+1}^2 \\
IS_2^4 = \;& u_{i-1}(547u_{i-1} - 2522u_i + 1922u_{i+1} - 494u_{i+2}) + u_i(3443u_i - 5966u_{i+1} \\
& +1602u_{i+2}) + u_{i+1}(2843u_{i+1} - 1642u_{i+2}) + 267u_{i+2}^2 \\
IS_3^4 = \;& u_i(2107u_i - 9402u_{i+1} + 7042u_{i+2} - 1854u_{i+3}) + u_{i+1}(11003u_{i+1} - 17246u_{i+2} \\
& +4642u_{i+3}) + u_{i+2}(7043u_{i+2} - 3882u_{i+3}) + 547u_{i+3}^2
\end{aligned} \tag{7}$$

The optimal weights are given by Balsara and Shu as [1],

$$C_0^4 = \frac{1}{35}, C_1^4 = \frac{12}{35}, C_2^4 = \frac{18}{35}, C_3^4 = \frac{4}{35} \tag{8}$$

and $\epsilon = 10^{-10},\ p = 2$. The optimum weights C_k will give the strict 7th order accuracy formulation defined by Eq.(3) that is symmetric about the interface being evaluated. For a Riemann solver such as the Roe scheme, the optimum weights C_k are the closest to the central differencing and hence generate the least numerical dissipation.

2.4 The New Seventh Order WENO Scheme

As aforementioned, the smoothness estimators IS_k^4 in Eq.(4) play two roles: One is that they can distinguish the stencils that contain discontinuities. The other role is that they are designed to have similar or uniform magnitude in smooth region so that the resulted scheme can give high order accuracy. IS_k^4 are not unique. As it is known mathematically, the derivatives can measure the smoothness of a function. Hence we may take a convex combination of derivatives as the smoothness estimators.

Herein, we propose a new smooth estimators IS_k^r defined by Eq.(9). For a function u given by discrete points, the lth order derivative $u_i^{(l)}$ can be replaced by finite differencing approximation, which is different from the lth undivided difference given by Liu et al.[2].

$$IS_k^r = \sum_{l=1}^{r-1} \beta_l [u_i^{(l)}(i+k-r+1, \cdots, i+k)\Delta x^l]^2 \tag{9}$$

where $u_i^{(l)}(i+k-r+1, \cdots, i+k)$ denotes the differencing approximation of lth order derivative $u_i^{(l)}$ by using points $x_{i+k-r+1}, \cdots, x_{i+k}$. Because r points are used, the highest order approximation of $u_i^{(l)}$ is $(r-l)$th order interpolation.

In fact, for the third-order($r = 2$) WENO scheme[2, 3], the smoothness measurements are

$$IS_0^2 = (u_{i+1} - u_i)^2, IS_1^2 = (u_{i+1} - u_i)^2, \tag{10}$$

One can obtain

$$\beta_1 = 1. \tag{11}$$

For fifth-order WENO($r=3$) scheme[3], the smoothness measurements are

$$\begin{aligned} IS_0^3 &= \tfrac{13}{12}(u_{i-2}-2u_{i-1}+u_i)^2+\tfrac{1}{4}(u_{i-2}-4u_{i-1}+3u_i)^2 \\ IS_1^3 &= \tfrac{13}{12}(u_{i-1}-2u_i+u_{i+1})^2+\tfrac{1}{4}(u_{i-1}-u_{i+1})^2 \\ IS_2^3 &= \tfrac{13}{12}(u_i-2u_{i+1}+u_{i+2})^2+\tfrac{1}{4}(3u_i-4u_{i+1}+u_{i+2})^2, \end{aligned} \tag{12}$$

One can obtain

$$\beta_1 = 1,\ \beta_2 = \frac{13}{12} \tag{13}$$

For the smoothness estimators Eq.(7) of seventh-order WENO($r=4$) scheme[1], we can have

$$\beta_1 = 240,\ \beta_2 = 1040,\ \beta_3 = 9732 \tag{14}$$

Obviously, the construction of the smoothness estimators in Eq.(7) and Eq.(14) are consistent with the definition given by Eq.(9) instead of Eq.(5).

The coefficients β_l (here, we only analyze the case with $r=4$) can affect the accuracy of the final scheme. For convenience, Table 1 lists the coefficients of $(u_{i+k+1-n}-u_{i+k-n})^2(\ n=1,\cdots,r-1)$ for different derivatives of power square (Due to the complexity resulted from the different '+' or '-' of the cross product terms, only the square-terms are analyzed in this paper. However, the conclusion is also applicable for the cross product terms in each IS_k). In Tables 1-3, the common denominator (36) is omitted. For $u_i^{(l)}(i+k-r+1,\cdots,i+k)$, it can always be expressed as a linear combination of $(u_{i+k+1-n}-u_{i+k-n})$. For example, if $k=0$,

$$\begin{aligned} u_i^{(1)}(i-3,\cdots,i) &= \tfrac{1}{6\Delta x}[11(u_i-u_{i-1})-7(u_{i-1}-u_{i-2})+2(u_{i-2}-u_{i-3})]+O(\Delta x^3) \\ u_i^{(2)}(i-3,\cdots,i) &= \tfrac{1}{2\Delta x^2}[2(u_i-u_{i-1})-3(u_{i-1}-u_{i-2})+(u_{i-2}-u_{i-3})]+O(\Delta x^2) \\ u_i^{(3)}(i-3,\cdots,i) &= \tfrac{1}{6\Delta x^3}[u_i-u_{i-1})-2(u_{i-1}-u_{i-2})+(u_{i-2}-u_{i-3})]+O(\Delta x) \end{aligned}$$

To measure the variation of the smoothness estimators, we define three parameters $RMXC$, $RMNC$ and MRC as:

$$RMXC = max(\delta m_0,\delta m_1,\delta m_2,\delta m_3)/min(\delta m_0,\delta m_1,\delta m_2,\delta m_3), \tag{15}$$

$$RMNC = max(\delta n_0,\delta n_1,\delta n_2,\delta n_3)/min(\delta n_0,\delta n_1,\delta n_2,\delta n_3), \tag{16}$$

and

$$MRC = max(RC_{-3},RC_{-2},\cdots,RC_2), \tag{17}$$

where δm_k is the maximum coefficient of $(u_{i+k+1-n}-u_{i+k-n})^2$ in IS_k^4, δn_k is the minimum coefficient of $(u_{i+k+1-n}-u_{i+k-n})^2$ in IS_k^4, $n=1,2,3$, and $k=0,...,3$. RC_j is the ratio of the maximum coefficient and the minimum coefficient of the same $(u_{i+j+1}-u_{i+j})^2, (j=-3,-2,\cdots,2)$ in different $IS_k^4(k=0,\cdots,3)$.

If the $RMXC$ and $RMNC$ are close to 1, the different $(u_{i+k+1-n}-u_{i+k-n})^2$ will have more uniform weight contribution. A smaller MRC means that the $(u_{i+j+1}-u_{i+j})^2$ has more the same effect on IS_k^4. This is very desirable to achieve the high accuracy in smooth region. For example, if one of $(u_{i+j+1}-u_{i+j})^2$ is much larger than the others, its contribution in the corresponding IS_k^4 will be amplified to MRC times. A larger MRC leads to a greater magnitude difference among IS_k^4, which will shift the weights away from the optimal weights C_k^r.

Table 2 gives the coefficients of $(u_{i+j+1}-u_{i+j})^2$ in IS_k^4 of Balsara and Shu's WENO-7[1]. One can easily get the ratios of this scheme as

$$RMXC = 133488/52848 \simeq 2.53,$$

$$RMNC = 19692/9612 \simeq 2.05,$$

and

$$MRC = max(133488/9612, 75852/19692, 75852/19692, 133488/9612) = 13.89$$

That is to say, even if the function is smooth, the weights calculated by IS_k^4 will not have the same contribution. This will reduce symmetry of the WENO scheme to make it deviate from the optimal differencing in the smooth region, which will be shown later by the numerical examples(See Tables 5 and 6 in Section 3).

Because the first order derivative of a function denotes the gradient and the second order derivative denotes the curvature, the convex combination of the 1st and 2nd order derivatives hence can basically measure the smoothness of a function. On the other hand, when a function is smooth, it is desirable that each $(u_{i+k} - u_{i+k-1})^2$ plays a uniform role. Such effect can be obtained by adjusting the coefficient of the third order derivative.

Without losing generality, let β_1 takes the value of 1. Fig. 1 gives the variations of $RMXC$ and $RMNC$ vs β_2 and β_3. It can be seen that the ratios become larger with increased β_2. When β_3 increases, the ratios approach to 1. Fig. 2 shows that MRC approaches to 4 when β_3 increases.

In smooth regions, Taylor expansion of IS_k^4 gives,

$$IS_k^4 = \beta_1(u_i^{'}\Delta x + O(\Delta x^4))^2 + \beta_2(u_i^{''}\Delta x^2 + O(\Delta x^4))^2 + \beta_3(u_i^{'''}\Delta x^3 + O(\Delta x^4))^2 \tag{18}$$

If $u^{'} \neq 0$, then

$$IS_k^4 = \beta_1(u^{'}\Delta x)^2(1 + O(\Delta x^2)) \tag{19}$$

When $u^{'} = 0$, we have

$$IS_k^4 = \beta_2(u^{''}\Delta x^2)^2(1 + O(\Delta x^2)) \tag{20}$$

In order to prevent the contribution of $u_i^{'''}$ from overwhelming that of $u_i^{'}$, we suggest $\beta_3 < \beta_1/\Delta x^4$.

In this paper, we take

$$\beta_1 = \beta_2 = 1, \beta_3 = 1000.$$

It can be seen that $RMXC$ and $RMNC$ are close to 1 and MRC is about 4 as shown in Figs. 1 and 2. Table 4 compares these ratios of the B-S and the present WENO schemes. These parameters indicate that the current 7th order WENO scheme will have more uniform smooth estimators in the smooth region, which will result in lower numerical dissipation and better accuracy in the smooth region than that of the WENO scheme of B-S[1].

3 Results and Discussion

Several numerical examples are used to demonstrate the accuracy of the new WENO-7 scheme proposed in this paper.

The fourth-order Runge-Kutta method[16] is applied for the unsteady examples in sections (3.1)-(3.5).

$$\begin{aligned} u^{(1)} &= u^n + \tfrac{1}{2}\Delta t L(u^n) \\ u^{(2)} &= u^n + \tfrac{1}{2}\Delta t L(u^{(1)}) \\ u^{(3)} &= u^n + \Delta t L(u^{(2)}) \\ u^{(4)} &= \tfrac{1}{3}(-u^n + u^{(1)} + 2u^{(2)} + u^{(3)}) + \tfrac{1}{6}\Delta t L(u^{(3)}) \end{aligned} \tag{21}$$

where $L(u)$ is the discretization of the spatial operator.

3.1 Linear Wave Equation

$$\frac{\partial u}{\partial t} + \frac{\partial u}{\partial x} = 0, -1 \leq x \leq 1 \tag{22}$$

3.1.1 Case 1

The test case 1 for the linear wave equation has the initial solution as

$$u_0(x) = sin(\pi x),$$

the domain in space is $(-1, 1)$ with periodic boundary condition imposed at the two ends.

Table 5 gives the accuracy order comparison at $t = 1$. Table 5 shows that the new scheme converges to 9th order accuracy for L_1 error and more than 7th order accuracy for L_∞ error, while the B-S 7th WENO scheme converges only slightly higher than 5th order accuracy for L_1 and 6th order for L_∞.

3.1.2 Case2

Case 2 uses the same linear wave equation, eq.(22), but the initial solution has two waves as

$$u_0(x) = sin(2\pi x).$$

Table 6 gives the comparison of the accuracy order measured at $t = 1$. Table 6 indicates that the new 7th order scheme converges to close to 7th order accuracy solution when the mesh is refined, while the B-S scheme only converges to 5th order accuracy and has not achieved the intended 7th order accuracy.

3.1.3 Case3

Case 3 again uses the same linear wave equation, eq.(22), the initial solution is given as

$$u_0(x) = \begin{cases} \frac{1}{6}[G(x,\beta,z-\delta) + G(x,\beta,z+\delta) + 4G(x,\beta,z)] & -0.8 \leq x \leq -0.6 \\ 1 & -0.4 \leq x \leq -0.2 \\ 1 - |10(x-0.1)| & 0.0 \leq x \leq 0.2 \\ \frac{1}{6}[F(x,\alpha,\alpha-\delta) + F(x,\alpha,\alpha+\delta) + 4F(x,\alpha,\alpha)] & 0.4 \leq x \leq 0.6 \\ 0 & otherwise \end{cases} \tag{23}$$

where

$$G(x,\beta,z) = e^{-\beta(x-z)^2}$$
$$F(x,\alpha,\alpha) = \sqrt{max(1-\alpha^2(x-\alpha)^2, 0)}$$

The constants are given by

$$\alpha = 0.5, z = -0.7; \delta = 0.005; \alpha = 10; \beta = \frac{log2}{36\delta^2}$$

Again, the periodic boundary condition is imposed at two ends. Fig. 3 gives the numerical comparison of B-S's WENO-7 and the new scheme with the grid $N = 200$. The new scheme can capture discontinuities very well, and has better accuracy than B-S WENO-7 scheme to resolve the wave peak as shown in Fig. 4.

3.2 The Burgers Equation

$$\frac{\partial u}{\partial t} + \frac{\partial u^2}{\partial x} = 0, 0 \leq x \leq 2\pi \tag{24}$$

with initial condition

$$u(x,0) = 0.3 + 0.7 * sin(x), periodic\ boundary\ condition$$

Figs. 5 gives the numerical comparison of B-S WENO-7 and the new scheme at $t = 2$. Both schemes capture the discontinuities very well. Fig. 6 is the zoomed region at the beginning of the discontinuity. It shows that the B-S scheme is slightly more diffusive.

3.3 The Viscous Burgers Equation

$$\frac{\partial u}{\partial t} + \frac{\partial u^2}{\partial x} = \mu \frac{\partial^2 u}{\partial x^2}, -1 \leq x \leq 1 \tag{25}$$

with the steady state boundary condition

$$u(-1) = tanh(0.5/\mu), u(1) = tanh(-0.5/\mu), \mu = 0.01$$

Fig. 7 shows the steady state solution of B-S WENO-7 and the new scheme. Both schemes agree with the analytical results very well. Fig. 8 is the zoomed region at the beginning of the discontinuity. It again shows that the new scheme is closer to the analytical solution and is less diffusive.

3.4 1D Shock Wave Tube, Sod Problem

The governing equation is one-dimensional Euler equations,

$$\frac{\partial \mathbf{U}}{\partial t} + \frac{\partial \mathbf{F}}{\partial x} = 0 \tag{26}$$

where

$$\mathbf{U} = \begin{bmatrix} \rho \\ \rho u \\ \rho e \end{bmatrix} \mathbf{F} = \begin{bmatrix} \rho u \\ \rho u^2 + p \\ u(\rho e + p))^T \end{bmatrix}, p = (\gamma - 1)(\rho e - \rho u^2/2),\ \gamma = 1.4.$$

The initial condition is

$$(\rho, u, p) = \begin{cases} (1.0, 0.0, 1.0), & x \leq 7.5, \\ (0.125, 0.0, 0.1), & x > 7.5. \end{cases} \tag{27}$$

The grid points is $N = 200$. Figs. 9 and 10 give the density and velocity distribution. Except a little oscillation near the contact discontinuity, the new scheme is good as the original scheme.

3.5 The Shu-Osher 1-D Shock Tube Problem

The governing equation is one-dimensional Euler equations (26), and the initial condition is

$$(\rho, u, p) = \begin{cases} (3.857143, 2.629369, 10.3333), & x < -4, \\ (1 + \varepsilon sin(5x), 0, 1), & x \geq -4. \end{cases}$$

This test case is taken from Ref.[16]. It represents a Mach 3 shock wave interacting with a sine entropy wave. Fig. 11 is the comparison of the density of the fifth-order WENO of Jiang and Shu, the seventh-order

WENO of B-S, and the new seventh-order WENO. Fig. 12 is the zoomed plot in the oscillation region behind the shock. Fig. 12 indicates that the 7th order reconstruction obtains much better resolution than the 5th order WENO scheme. The new 7th order WENO resolves the wave amplitude significantly better than the B-S WENO scheme with less dissipation.

3.6 Subsonic Flat Plate Turbulent Boundary Layer

To test the new 7th order WENO scheme for multi-dimensional flows, several 2D cases are calculated. The implicit unfactured Gauss-Seidel Relaxation scheme is used for time marching[11]. The strategy of using $\varepsilon = 10^{-2)}$ for WENO scheme as suggested in [11] is used. The Roe's flux difference scheme [17] is used as the Riemann solver with the WENO scheme for the multi-dimensional calculation in this paper.

The subsonic flat plate turbulent boundary layer is used as the first 2-D test example. In this case, the Baldwin-Lomax turbulence model is used. The computation domain is taken to be $[0,1] \times [0,1]$. The cell size is 180×80. The non-dimensional distance y^+ of the first point to the wall is kept under 0.2. The inlet Mach number is 0.5, and the Reynolds number is 4×10^6 based on the plate length. The flow is subsonic at inlet and outlet. The CFL number of 200 is used.

Fig. 13 shows that the results of both the 7th-order WENO schemes agree well with the law of the wall. Fig. 14 shows that the new scheme has the same convergence as the B-S scheme.

3.7 Transonic Converging-Diverging Nozzle

To examine the performance of the new 7th order WENO scheme for capturing the weak shock waves that do not align with the mesh lines, an inviscid transonic converging-diverging nozzle is calculated. The nozzle was designed and tested at NASA and was named as Nozzle A2[18]. The cell size is 175×80. The grid is clustered near the wall. The inlet Mach number is 0.22.

Fig. 15 is the pressure contours. Fig. 16 is the distribution of the wall pressure coefficient. It can be seen that present scheme obtained sharper peak than Balsara and Shu's WENO schemes. Though there is a small oscillation, the result is acceptable.

3.8 Transonic RAE2822 Airfoil

The steady state solution of the transonic RAE2822 airfoil is calculated using the new 7th order WENO scheme with Reynolds averaged NS equation. The Baldwin-Lomax turbulent model is used. The computational region is divided into two blocks, and the mesh size of 128×55 is used for each block, the freestream Mach number M_∞ is 0.729, the Reynolds number based on chord is 6.5×10^6, and the angle of attack is 2.31^o.

Fig. 17 is the pressure contours showing the shock captured on the suction surface. Fig. 18 is the comparison of the pressure coefficients. Both results are in good agreement with the experiment.

4 Conclusions

An improved smoothness estimator to construct the weights for 7th order WENO scheme is proposed in this paper. The suggested smoothness estimators have less variation than the B-S formulation and hence generate the weights closer to the optimal ones with less numerical dissipation. The numerical experiment shows that the new WENO scheme not only can capture the shock well, but can also obtain higher accuracy than the original B-S 7th order WENO scheme. Since only the coefficients of the smoothness estimator are

modified, the improved WENO scheme has the same computational efficiency as the B-S WENO scheme. The new 7th order WENO scheme is also applied to 2-dimensional transonic flows to demonstrate its robustness.

5 Acknowledgment

This work is partially supported by AFOSR Grant F49620-03-1-0253 monitored by Dr Fariba Fahroo, by ARO grant 56827-RT-ISP monitored by Lt Col. R. Jefferies at AFOSR and J. Haire at ARO, and by Miami Wind at University of Miami.

References

[1] D.S. Balsara and C.-W. Shu, "Monotonicity Preserving weighted essentially non-oscillatory schemes with increasingly high order of accuracy," *J.Comput.Phys.*, vol. 160, pp. 405–452, 2000.

[2] X.D. Liu, S. Osher, and T. Chan, "Weighted essentially non-oscillatory schemes," *J.Comput.Phys.*, vol. 126, pp. 200–212, 1994.

[3] G.S. Jiang, and C.W. Shu, "Efficient implementation of weighted ENO schemes," *J.Comput.Phys.*, vol. 126, pp. 202–228, 1996.

[4] C.-W. Shu, "High-order finite difference and finite volume WENO schemes and discontinuous galerkin methods for CFD," *Inter.J.Comput.Fluid.Dyn.*, vol. 17, pp. 107–118, 2003.

[5] Z.J. Wang and R.F. Chen, "Optimized weighted essentially non-oscillatory schemes for linear waves with discontinuity," *J.Comput.Phys.*, vol. 174, pp. 381–404, 2001.

[6] D. Ponziani, S. Pirozzoli, F. Grasso, "Development of optimized weighted-ENO schemes for multiscale compressible flows," *Inter.J.Numer.Meth.Fluids*, vol. 42, pp. 953–977, 2003.

[7] Z.F. Xu and C.-W. Shu, "Anti-diffusive flux corrections for high order finite difference WENO schemes," *J.Comput.Phys.*, vol. 205, pp. 458–485, 2005.

[8] A.K. Henrick, T.D. Aslam, J.M. Powers, "Mapped weighted essentially non-oscillatory schemes:Achiving optimal order near critical points," *J.Comput.Phys.*, vol. 208, pp. 206–227, 2005.

[9] S. Pirozzoli, "Conservative hybrid compact-WENO schemes for shock-turbulence interaction," *J.Comput.Phys.*, vol. 178, pp. 81–117, 2002.

[10] D. Kim and J.H. Kwon, "A high-order accurate hybrid scheme using a central flux scheme and a WENO scheme for compressible flowfield analysis," *J.Comput.Phys.*, vol. 210, pp. 554–583, 2005.

[11] Y.Q. Shen and G.W. Yang, "Hybrid finite compact-WENO schemes for shock calculation," *Interational Journal for Numerical Methods in Fluids*, vol. 53, pp. 531–560, 2007.

[12] M. Latini, O. Schilling, W.S. Don, "Effects of WENO flux reconstruction order and spatial resolution on reshocked two-dimensional Richmyer-Meshkov instability," *J.Comput.Phys.*, vol. 221, pp. 805–836, 2007.

[13] B.van Leer, "Towards the ultimate conservative difference scheme, v:a second-order sequel to godunov's method," *J. Compu. Phys.*, vol. 32, pp. 101–136, 1979.

[14] C.Q. Liu, L. Jiang, M. Visbal, P. Xie, " Smart weigthed compact scheme for shock tube and shock-entropy interaction ." AIAA-2006-3708, 2006.

[15] Y.Q. Shen, B.Y. Wang,and G.C. Zha, "Implicit WENO scheme and high order viscous formulas for compressible flows." AIAA-paper 2007-4431, June 2007.

[16] C.-W. Shu and O. Osher, "Efficient Implementation of Essentially Non-Oscillatory Shock Capturing Schemes," *Journal of Computational Physics*, vol. 77, pp. 439–471, 1988.

[17] P. Roe, "Approximate Riemann Solvers, Parameter Vectors, and Difference Schemes," *Journal of Computational Physics*, vol. 43, pp. 357–372, 1981.

[18] M. L. Mason and L. E. Putnam, "The Effect of Throat Contouring on Two-Dimensional Converging-Diverging Nozzles at Static Conditions ." NASA Technical Paper 1704, 1980.

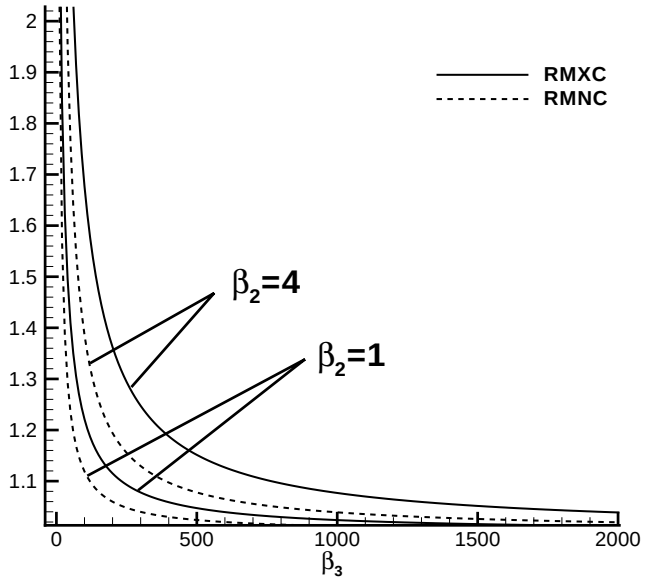

Figure 1: Variation of RMXC and RMNC

Table 1: The coefficients of $(u_{i+l+1} - u_{i+l})^2$ in different derivatives

	$(u_{i-2} - u_{i-3})^2$	$(u_{i-1} - u_{i-2})^2$	$(u_i - u_{i-1})^2$	$(u_{i+1} - u_i)^2$	$(u_{i+2} - u_{i+1})^2$	$(u_{i+3} - u_{i+2})^2$
$(u_i^{'''})^2$	1	4	1			
$(u_i^{''})^2$	9	81	36			
$(u_i^{'})^2$	4	49	121			
$(u_i^{'''})^2$		1	4	1		
$(u_i^{''})^2$		0	9	9		
$(u_i^{'})^2$		1	25	4		
$(u_i^{'''})^2$			1	4	1	
$(u_i^{''})^2$			9	9	0	
$(u_i^{'})^2$			4	25	1	
$(u_i^{'''})^2$				1	4	1
$(u_i^{''})^2$				36	81	9
$(u_i^{'})^2$				121	49	4

Table 2: The coefficients of $(u_{i+l+1} - u_{i+l})^2$ in IS_k^4 of B-S WENO-7

	$(u_{i-2} - u_{i-3})^2$	$(u_{i-1} - u_{i-2})^2$	$(u_i - u_{i-1})^2$	$(u_{i+1} - u_i)^2$	$(u_{i+2} - u_{i+1})^2$	$(u_{i+3} - u_{i+2})^2$
	9372	37488	9372			
IS_0^4	9360	84240	37440			
	960	11760	29040			
$\sum$	19692	133488	75852			
		9372	37488	9372		
IS_1^4		0	9360	9360		
		240	6000	960		
$\sum$		9612	52848	19692		
			9372	37488	9372	
IS_2^4			9360	9360	0	
			960	6000	240	
$\sum$			19692	52848	9612	
				9372	37488	9372
IS_3^4				37440	84240	9360
				29040	11760	960
$\sum$				75852	133488	19692

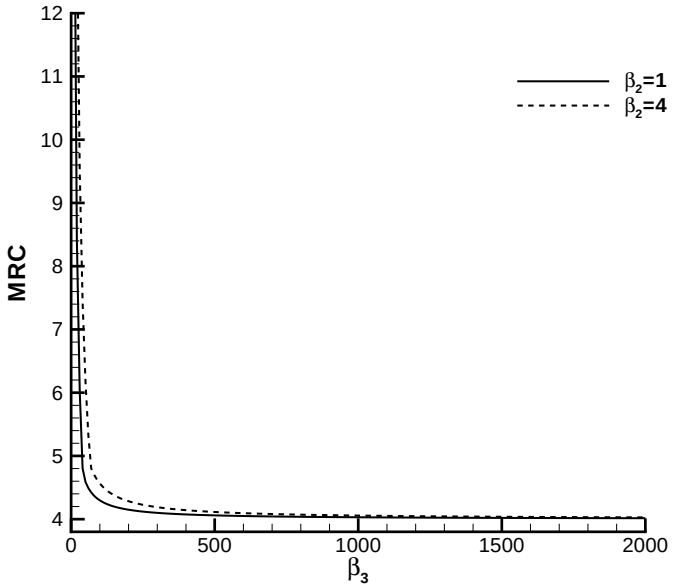

Figure 2: Variation of MRC

Table 3: The coefficients of $(u_{i+l+1}-u_{i+l})^2$ in IS_k^4 of the new WENO-7

	$(u_{i-2}-u_{i-3})^2$	$(u_{i-1}-u_{i-2})^2$	$(u_i-u_{i-1})^2$	$(u_{i+1}-u_i)^2$	$(u_{i+2}-u_{i+1})^2$	$(u_{i+3}-u_{i+2})^2$
IS_0^4	1000	4000	1000			
	9	81	36			
	4	49	121			
	1013	4130	1157			
IS_1^4		1000	4000	1000		
		0	9	9		
		1	25	4		
$\sum$		1001	4034	1013		
IS_2^4			1000	4000	1000	
			9	9	0	
$\sum$			4	25	1	
$\sum$			1013	4034	1001	
IS_3^4				1000	4000	1000
				36	81	9
				121	49	4
$\sum$				1157	4130	1013

Table 4: The parameters $RMXC$, $RMNC$ and MRC of B-S and the present WENO scheme

Scheme	RMXC	RMNC	MRC
B-S	2.53	2.05	13.89
Present	1.02	1.01	4.13

Table 5: Comparison of the accuracy order of $u_0(x) = sin(\pi x)$, $t = 1$

Method	Number	L_1 error	L_1 order	L_∞ error	L_∞ order
B-S WENO-7	40	0.297859E-05	——	0.608510E-06	——
	80	0.816595E-07	5.189	0.944894E-08	6.010
	160	0.229575E-08	5.153	0.145473E-09	6.021
	320	0.640233E-10	5.164	0.233123E-11	5.964
	640	0.158740E-11	5.334	0.311898E-13	6.224
New	40	0.479162E-05	——	0.863755E-06	——
	80	0.128698E-06	5.218	0.134466E-07	6.005
	160	0.274376E-08	5.552	0.169079E-09	6.313
	320	0.230745E-10	6.894	0.115607E-11	7.912
	640	0.344169E-13	9.389	0.574858E-14	7.652

Table 6: Comparison of the accuracy order of $u_0(x) = sin(2\pi x)$, $t = 1$

Method	Number	L_1 error	L_1 order	L_∞ error	L_∞ order
B-S WENO-7	40	0.225660E-03	—	0.851062E-04	—
	80	0.541236E-05	5.382	0.122066E-05	6.124
	160	0.148030E-06	5.192	0.184773E-07	6.046
	320	0.414090E-08	5.160	0.282285E-09	6.032
	640	0.114947E-09	5.171	0.443706E-11	5.991
New	40	0.120874E-02	—	0.469407E-03	—
	80	0.104767E-04	6.850	0.210932E-05	7.798
	160	0.226829E-06	5.529	0.265730E-07	6.311
	320	0.488307E-08	5.538	0.325087E-09	6.353
	640	0.441225E-10	6.790	0.231720E-11	7.132

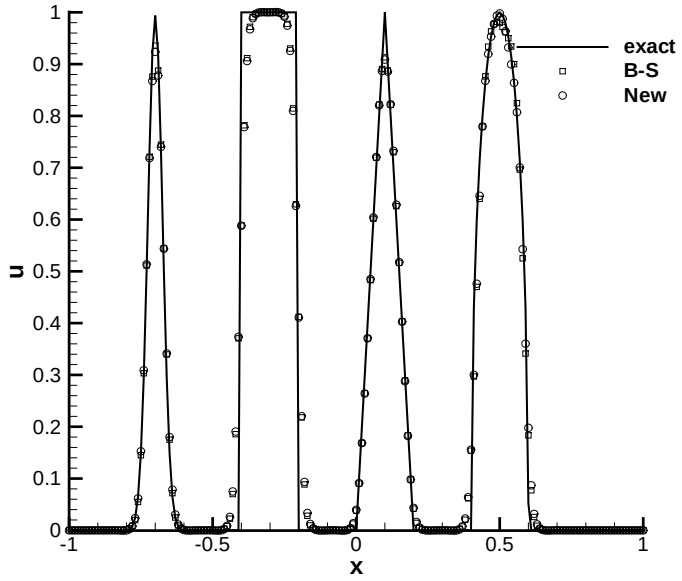

Figure 3: Numerical results of case 3 computed by the linear wave equation using 7th order WENO schemes

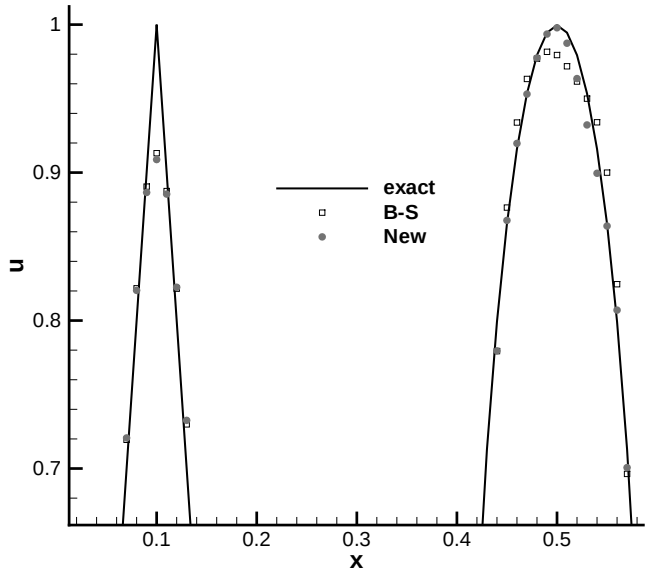

Figure 4: Zoomed plot of the wave peak computed by 7th order WENO schemes

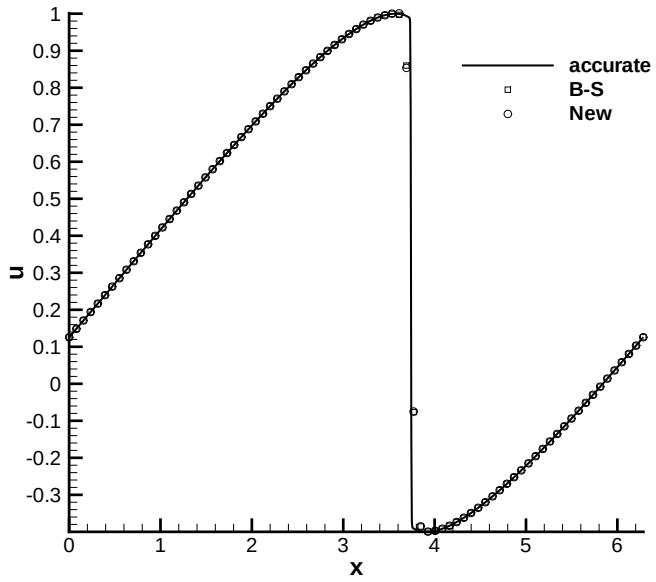

Figure 5: Computed results of the Burgers equation using 7th order WENO schemes

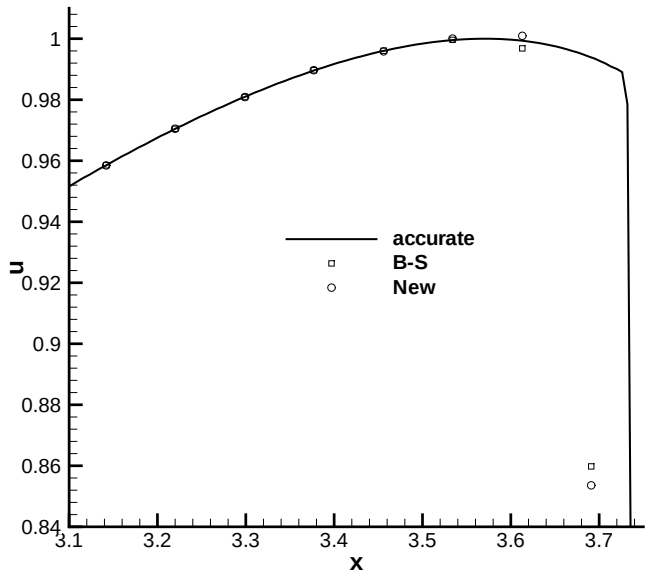

Figure 6: Zoomed region at the begin of the discontinuity

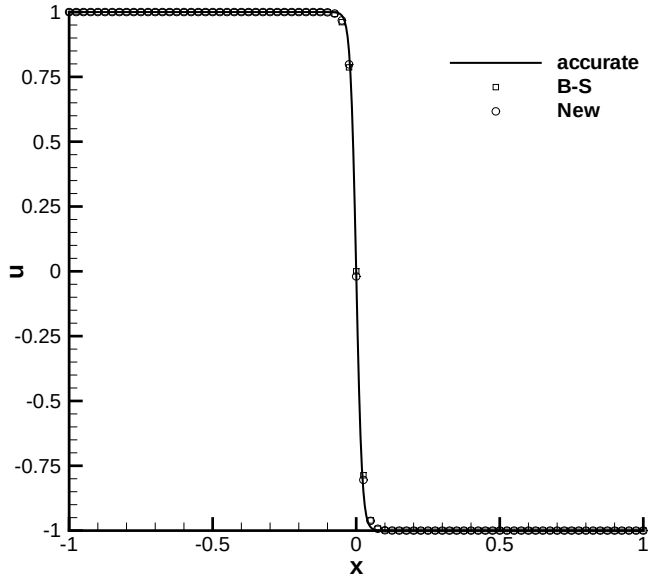

Figure 7: Numerical results of the viscous Burgers equation computed by using 7th order WENO scheme

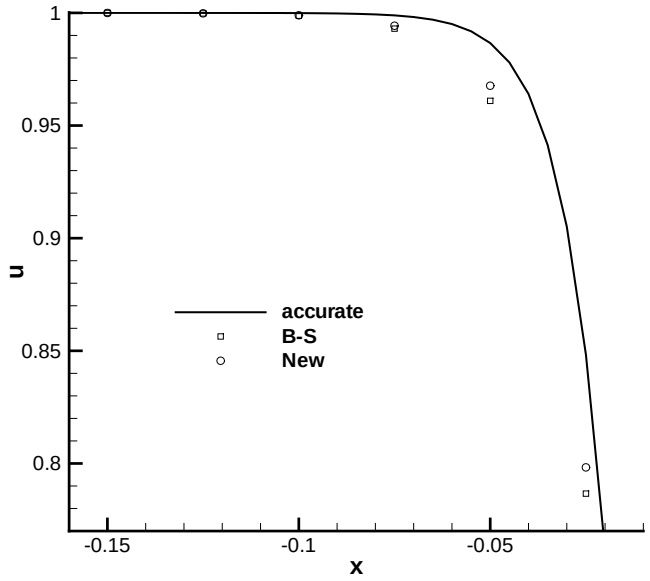

Figure 8: Zoomed region at the begin of the computed discontinuity

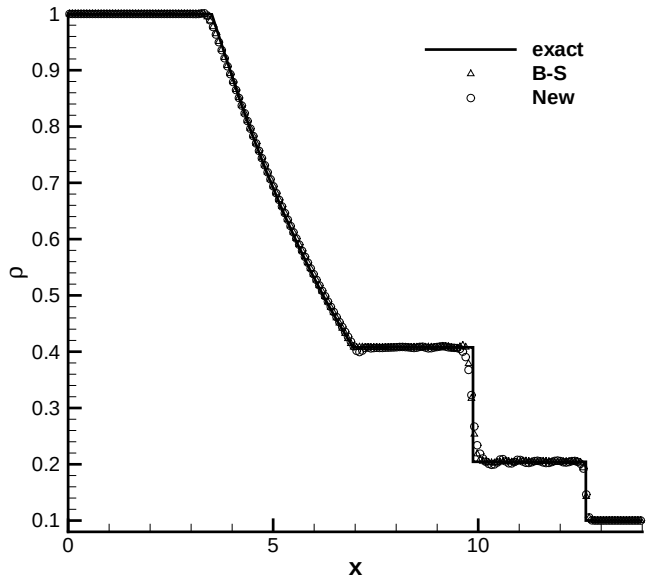

Figure 9: Density distribution of Sod's problem

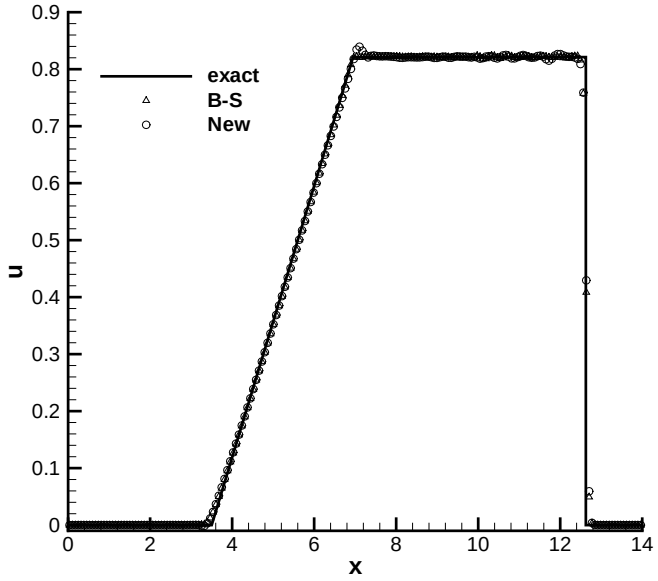

Figure 10: Velocity distribution of Sod's problem

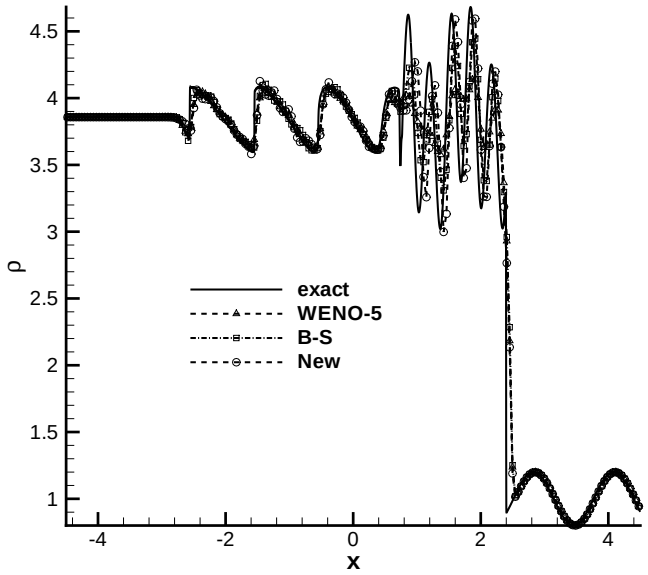

Figure 11: Density distribution of Shu-Osher's problem computed by using different WENO schemes

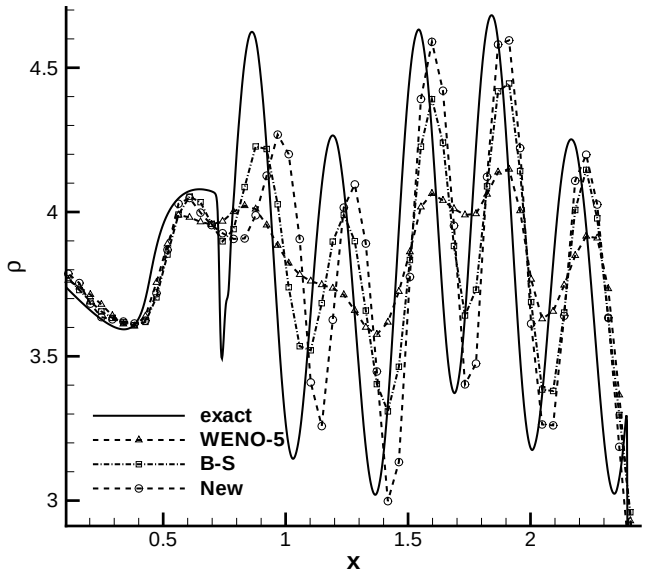

Figure 12: Zoomed region of the wave oscillation behind the shock for the Shu-Osher 1D shock tube problem

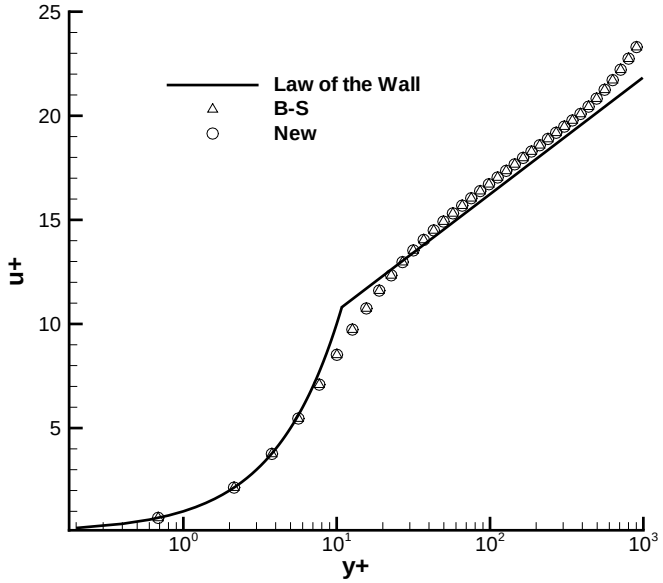

Figure 13: The velocity profiles of the supersonic laminar boundary layer flow.

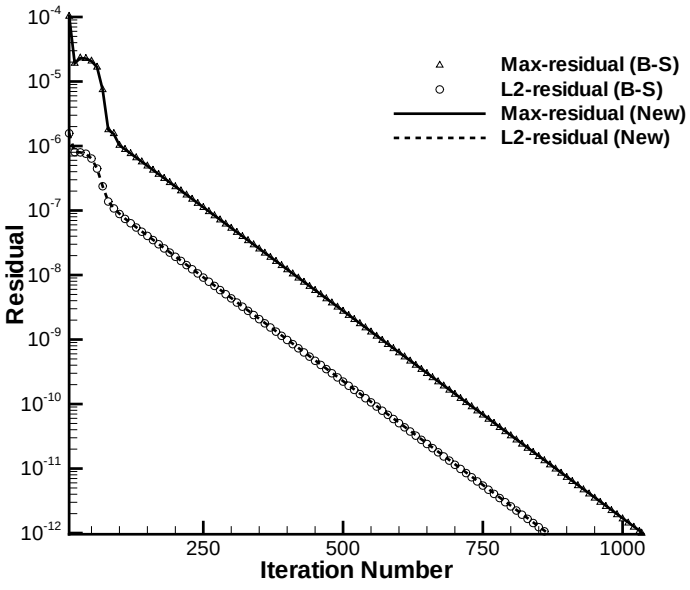

Figure 14: Convergence history of the supersonic laminar boundary layer flow.

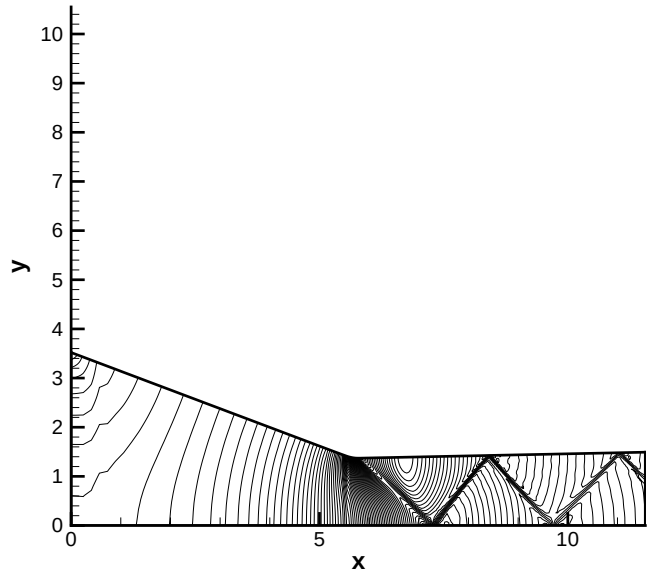

Figure 15: Pressure contours of Nozzle A2 computed by using the Euler equations with the new 7th order WENO scheme

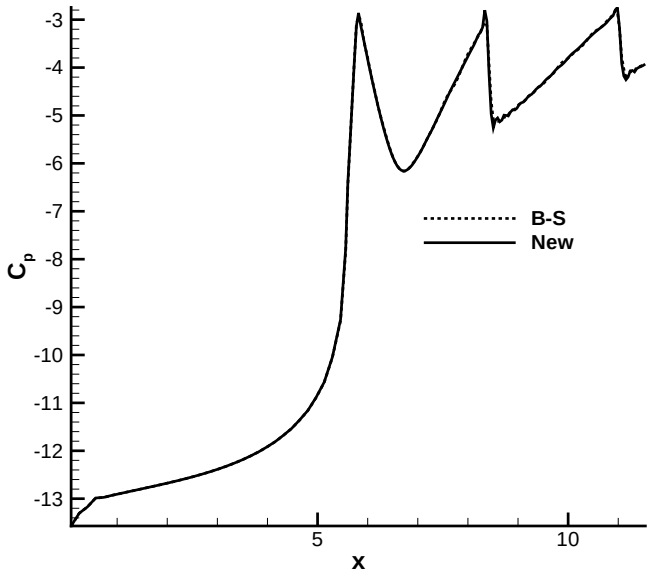

Figure 16: Comparison of the wall pressure coefficient of Nozzle A2 computed by using the Euler equations

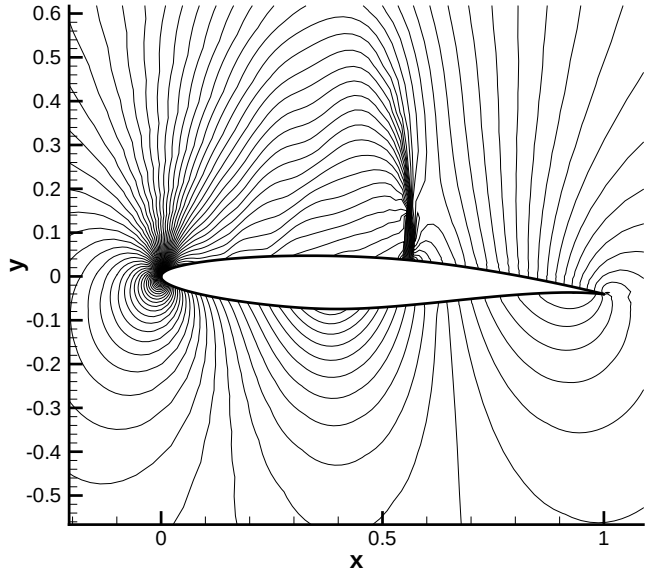

Figure 17: Pressure contours of RAE2822 computed using the new 7th order WENO scheme

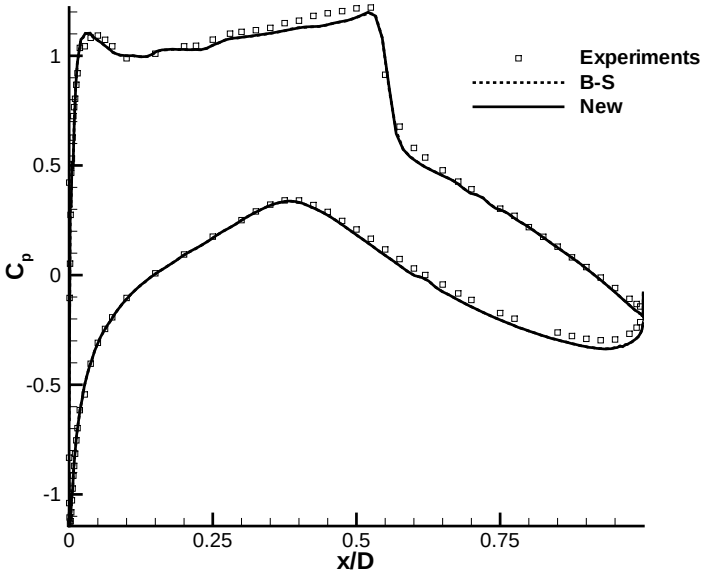

Figure 18: Comparison of the wall pressure coefficient of RAE2822